

Is quantum frequency entanglement between signal-idler pairs generated in a biphoton source necessary for observing induced coherence between signal photons generated in separate sources?

Arturo Rojas-Santana*

*ICFO - Institut de Ciències Fotoniques, The Barcelona Institute of Science and Technology, 08860 Castelldefels (Barcelona), Spain and
Tecnologico de Monterrey, Escuela de Ingeniería y Ciencias,
Ave. Eugenio Garza Sada 2501, Monterrey, N.L. 64849, Mexico*

Gerard J. Machado

ICFO - Institut de Ciències Fotoniques, The Barcelona Institute of Science and Technology, 08860 Castelldefels (Barcelona), Spain

Dorilian Lopez-Mago

*Tecnologico de Monterrey, Escuela de Ingeniería y Ciencias,
Ave. Eugenio Garza Sada 2501, Monterrey, N.L. 64849, Mexico*

Juan P. Torres

*ICFO - Institut de Ciències Fotoniques, The Barcelona Institute of Science and Technology, 08860 Castelldefels (Barcelona), Spain and
Departament of Signal Theory and Communications,
Universitat Politècnica de Catalunya, 08034 Barcelona, Spain*

(Dated: May 7, 2022)

There is renewed interest in using the coherence between beams generated in separate down-converter sources for new applications in imaging, spectroscopy, microscopy and optical coherence tomography (OCT). These schemes make use of continuous wave (CW) pumping in the low parametric gain regime, which generates frequency entanglement between the signal-idler pairs generated in a single source. Is this frequency entanglement a requisite to observe coherence between signal photons generated in separate biphoton sources? We will show that it is not. This might be an advantage for OCT applications. High axial resolution requires a large bandwidth. For CW pumping this requires the use of short nonlinear crystals. This is detrimental since short crystals generate small photon fluxes. We show that the use of ultrashort pump pulses allows improving axial resolution even for long crystal that produce higher photon fluxes.

I. INTRODUCTION

In 1991 Zou et al. [1, 2] demonstrated that indistinguishability of idler beams generated at separate parametric down-converting sources can *induce coherence* between the signal beams generated at the same separate sources. The effect was demonstrated originally at the low parametric gain regime, where the probability to generate pairs of photons simultaneously in each source is very low. However coherence is also observed in the high parametric gain regime [3, 4]. Here we are interested in the low parametric gain regime, since this scenario allows to quantify the degree of entanglement between down-converted photons straightforwardly.

Induced coherence in a system of two parametric down-converters is a particular case of a broader class of interferometers sometimes referred as *nonlinear interferometers* [7] based on optical parametric amplifiers. The last few years have seen a surge of interest in using these interferometers for new schemes in imaging [8, 9], sensing

[10], spectroscopy [11, 12], microscopy [13, 14] and OCT [15–18]. One advantage of these systems is that one can choose a wavelength for the beam that interacts with the sample and is never detected, and another wavelength for the beam to be detected that enhance photo-detection efficiency. They also can show better sensitivity than alternative schemes [19, 20].

Up to now all experiments but two [15?] are performed in the low parametric gain regime. In all these cases the bandwidth of the pump laser (δ_p) is considerably smaller than the bandwidth of down-conversion (Δ_{dc}) [21]. This produces a high degree of entanglement between signal and idler beams generated in a single biphoton source. The entropy of entanglement [22], that is a quantitative measure of how much entanglement there is between signal and idler photons generated, is large when the ratio $\Delta_{dc}/\delta_p \gg 1$ or $\Delta_{dc}/\delta_p \ll 1$.

This can lead to think that frequency entanglement between signal-idler pairs generated in a nonlinear crystal is a necessary condition to observe induced coherence between signal photons generated in separate nonlinear crystals. We will demonstrate below that induced coherence happens when there is no frequency entanglement

* jorge-arturo.rojas@icfo.eu

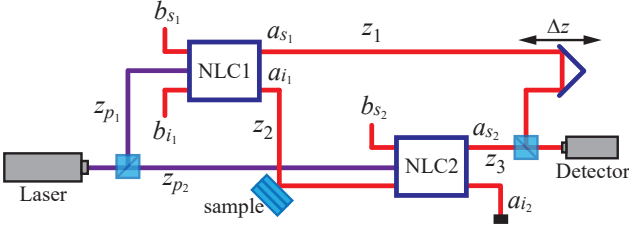


FIG. 1. Induced coherence between signal photons generated in separate parametric down-converters. The idler traverses a lossy sample before being injected into NLC₂. The detector measures the interference between signal photons s_1 and s_2 as a function of the path delay Δz . NLC: nonlinear crystal; s, i : signal and idler modes; b, a input/output quantum operators.

and even no correlations, so importantly CW pumping is not a requisite to observe induced coherence. As we will show, this can have important practical consequences for the implementation of high-flux and high-resolution optical coherence schemes based on induced coherence.

II. ROLE OF SIGNAL-IDLER ENTANGLEMENT FOR OBSERVING INDUCED COHERENCE

Figure 1 shows a scheme of an induced coherence experiment with two parametric down-converters (NLC₁ and NLC₂). We consider a pulsed laser that generates coherent light with a spectrum $F(\Omega_p)$. The frequency of the pump is $\omega_p = \omega_p^0 + \Omega_p$, with ω_p^0 being the central frequency and Ω_p the frequency deviation from the central frequency. A beam splitter divides the pump beam into two coherent sub-beams that pump the two nonlinear crystals. The two sub-beams travel distances z_{p1} and z_{p2} before reaching NLC₁ and NLC₂, respectively.

Both crystals have nonlinear susceptibility $\chi^{(2)}$ and length L . The nonlinear interaction generates signal and idler photons s_1 and i_1 in NLC₁, and s_2 and i_2 in NLC₂. The frequency of the signal and idler photons reads $\omega_s = \omega_s^0 + \Omega_s$ and $\omega_i = \omega_i^0 + \Omega_i$, where $\omega_{s,i}^0$ are central frequencies and $\Omega_{s,i}$ are frequency deviations from the corresponding central frequencies. The conditions $\omega_p^0 = \omega_s^0 + \omega_i^0$ and $\Omega_p = \Omega_s + \Omega_i$ are satisfied.

The quantum operators $a_{s1,s2}(\Omega_s)$ and $a_{i1,i2}(\Omega_i)$ correspond to signal and idler modes at the output face of the corresponding nonlinear crystals. $b_{s1,s2}(\Omega_s)$ and $b_{i1,i2}(\Omega_i)$ designate the corresponding operators at the input face. In the low parametric gain regime, the Bogoliubov transformations that relate the input-output operators for NLC₁ are [24, 25]:

$$a_{s1}(\Omega_s) = U_s(\Omega_s)b_{s1}(\Omega_s) + \int d\Omega_i V_{s1}(\Omega_s, \Omega_i)b_{i1}^\dagger(\Omega_i), \quad (1)$$

$$a_{i1}(\Omega_i) = U_i(\Omega_i)b_{i1}(\Omega_i) + \int d\Omega_s V_{i1}(\Omega_s, \Omega_i)b_{s1}^\dagger(\Omega_s), \quad (2)$$

where $U_s(\Omega_s) = \exp[ik_s(\Omega_s)L]$, $U_i(\Omega_i) = \exp[ik_i(\Omega_i)L]$

and

$$V_{s1}(\Omega_s, \Omega_i) = i(\sigma L)F_{p1}(\Omega_s + \Omega_i)\text{sinc}\left[\frac{\Delta k L}{2}\right] \times \exp\left[i\frac{k_p(\Omega_s + \Omega_i) + k_s(\Omega_s) - k_i(\Omega_i)}{2}L\right], \quad (3)$$

$$V_{i1}(\Omega_s, \Omega_i) = i(\sigma L)F_{p1}(\Omega_s + \Omega_i)\text{sinc}\left[\frac{\Delta k L}{2}\right] \times \exp\left[i\frac{k_p(\Omega_s + \Omega_i) + k_i(\Omega_i) - k_s(\Omega_s)}{2}L\right]. \quad (4)$$

The nonlinear coefficient σ is [21, 24, 25]

$$\sigma = \left[\frac{\hbar\omega_p^0\omega_s^0\omega_i^0[\chi^{(2)}]^2 N_0}{16\pi\epsilon_0 c^3 n_p n_s n_i A} \right]^{1/2}, \quad (5)$$

where N_0 is the number of pump photons per pulse, A is the effective area of interaction and $n_{p,s,i}$ are refractive indexes at the central frequencies of all waves involved. The function F_{p1} is

$$F_{p1}(\Omega_p) = \frac{T_0^{1/2}}{\pi^{1/4}} \exp\left[-\frac{\Omega_p^2 T_0^2}{2}\right] \exp[ik_p(\Omega_p)z_{p1}], \quad (6)$$

where we have assumed a Gaussian shape for the spectrum of the pump beam. The function F_p is normalized to 1. T_0 is the temporal width of the pump pulses. The wave-vector phase mismatch is $\Delta k = k_p(\Omega_s + \Omega_i) - k_s(\Omega_s) - k_i(\Omega_i)$. If we expand in Taylor series to first order the wave-vectors as $k_i(\Omega) = k_i^0 + N_i\Omega$ ($N_{p,s,i}$ are inverse group velocities) and assume perfect phase matching at the central frequencies ($k_p^0 = k_s^0 + k_i^0$), we obtain $\Delta k = D_+\Omega_p + D_-\Omega_-/2$, where $\Omega_- = \Omega_s - \Omega_i$, $D_+ = N_p - (N_s + N_i)/2$ and $D_- = N_i - N_s$.

The idler mode a_{i1} traverses a distance z_2 before encountering a lossy sample characterized by reflectivity $r(\Omega_i)$. The quantum operator transformation that describes this process is [26, 27]

$$a_{i1}(\Omega_i) \longrightarrow r(\Omega_i)a_{i1}(\Omega_i) \exp[ik_i(\Omega_i)z_2] + f(\Omega_i), \quad (7)$$

where the operator f fulfills the commutation relationship $[f(\Omega), f^\dagger(\Omega')] = (1 - |r(\Omega)|^2)\delta(\Omega - \Omega')$.

The idler beam is injected into NLC₂ so that the operator a_{s2} that describes signal beam s_2 at the output face of NLC₂ is

$$a_{s2}(\Omega_s) = U_s(\Omega_s)b_{s2}(\Omega_s) + \int d\Omega_i V_{s2}(\Omega_s, \Omega_i)f^\dagger(\Omega_i) \quad (8) \\ + \int d\Omega_i r^*(\Omega_i)V_{s2}(\Omega_s, \Omega_i)U_i^*(\Omega_i) \exp[-ik_i(\Omega_i)z_2]b_i^\dagger(\Omega_i),$$

where only terms up to first order in σL has been considered, the terms that give a non-zero contribution in the calculation of the first-order correlation function. The function V_{s2} is analogous to V_{s1} in Eq. (3) with $F_{p2} = F_p(\Omega_p) \exp[ik_p(\Omega_p)z_{p2}]$.

Signal photon s_1 traverses a distance z_1 before detection, and signal photon s_2 traverses a distance z_3 . The

number of signal photons generated per pulse, $N_{s_1} = \int d\Omega a_{s_1}^\dagger(\Omega) a_{s_1}(\Omega)$ and $N_{s_2} = \int d\Omega a_{s_2}^\dagger(\Omega) a_{s_2}(\Omega)$ is

$$N_{s_1} = N_{s_2} = 2\pi \frac{\sigma^2 L}{D}. \quad (9)$$

It depends on the total number of pump photons per pulse, however it is independent of the shape of the pulse. This fact and that $N_{s_1} = N_{s_2}$ are characteristics of the low parametric gain regime.

We are interested in the normalized first-order correlation function $g_{s_1, s_2}^{(1)}$ between beams s_1 and s_2 that gives the visibility of the interference fringes detected after combining both signals in a beam splitter, i.e.,

$$g_{s_1, s_2}^{(1)} = \frac{1}{N_{s_1}^{1/2} N_{s_2}^{1/2}} \int d\Omega a_{s_1}^\dagger(\Omega) a_{s_2}(\Omega). \quad (10)$$

Let us first assume that there are no losses in the idler path ($r(\Omega) = 1$). Using Eqs. (1), (8) and (9) into Eq. (10) and taking into account the distances z_1 and z_3 that signal beams s_1 and s_2 propagate before combination in the beam splitter, the first-order correlation function can be written as

$$\left| g_{s_1, s_2}^{(1)}(T_1, T_2) \right| = \text{tri} \left(\frac{T_1}{DL} \right) \times \exp \left[-\frac{1}{16T_0^2} \left[\left(1 - \frac{2D_+}{D} \right) T_1 + 2T_2 \right]^2 \right], \quad (11)$$

where $\text{tri}(\xi/2) = 1/\pi \int \text{sinc}^2(x) \exp(i\xi x) dx$ is the triangular function and

$$T_1 = \frac{z_3 - z_1 + z_2}{c} + N_i L, \quad (12)$$

$$T_2 = \frac{z_{p2} - z_{p1} - z_2}{c} - N_i L. \quad (13)$$

We assume that the condition $z_{p2} = z_{p1} + cN_i L + z_2$ is fulfilled, so that $T_2 = 0$. In order to optimize pulsed parametric amplification in NLC₂ one needs to synchronize the time of arrival of pump and idler pulses to the nonlinear crystal [15].

The first-order correlation function is the product of a triangular function of width DL and a Gaussian function of width T_0 . Figure 2 plots the first-order correlation function as a function of $\Delta z = z_3 - z_1 + z_2 + cN_i L$ for a crystal length $L = 5$ mm and three different pulse widths: $T_0 = 100$ ps, $T_0 = 2$ ps and $T_0 = 100$ fs. Δz can be modified in an experiment by changing the pathlength difference $z_3 - z_1$. We have considered as example two MgO-doped LiNbO₃ crystals [28] pumped by a pulsed laser operating at $\lambda_p^0 = 532$ nm. The resulting type-0 signal and idler beams have wavelengths $\lambda_s^0 = 810$ nm and $\lambda_i^0 = 1550$ nm with $D = -263.50$ fs/mm and $D_+ = 780$ fs/mm.

In the limiting case of CW pumping ($T_0 \rightarrow \infty$), the shape of the first-order correlation function is dominated by the triangular function [see Fig. 2(a)], as it has been measured in many occasions [16]. As we decrease the

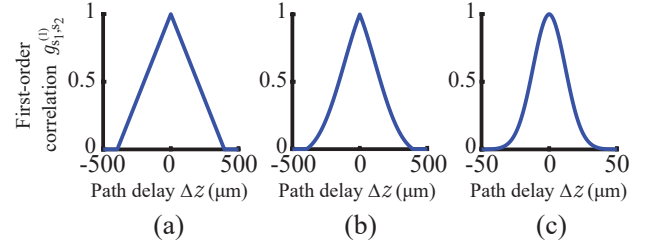


FIG. 2. First-order correlation function as a function of the path delay Δz . We consider a crystal with length $L = 5$ mm. The pump pulses have temporal widths: (a) $T_0 = 100$ ps; (b) $T_0 = 2$ ps; and (c) $T_0 = 100$ fs.

temporal width of the pump pulses, the influence of the triangular and Gaussian functions on $g_{s_1, s_2}^{(1)}$ becomes comparable [Fig. 2(b)]. Finally, when $T_0 \ll DL$, the shape of the first-order correlation function is dominated by the Gaussian function [Fig. 2(c)].

Is entanglement between signal and idler photons relevant for observing induced coherence? Inspection of Fig. 2 shows that it is not, since for all values of T_0 and crystal length L , that correspond to quantum states with different degrees of entanglement, there is induced coherence. For the sake of clarity, let us be more specific. In the low parametric gain regime, the biphoton function

$$\Psi(\Omega_s, \Omega_i) = i\sigma L F(\Omega_s + \Omega_i) \text{sinc} \left[\frac{\Delta k L}{2} \right] \exp(i s_k L), \quad (14)$$

where $s_k = k_p(\Omega_s + \Omega_i) + k_s(\Omega_s) + k_i(\Omega_i)$, determines the nature of the correlations between the paired photons and the degree of entanglement between them [25]. If we can decompose $\Psi(\Omega_s, \Omega_i)$ into two functions that depend separately on the variables Ω_s and Ω_i the quantum state is non-entangled (separable).

For the sake of simplicity, let us consider $D_+ = 0$ and make the approximation $\text{sinc}(x) \sim \exp(-\alpha^2 x^2)$ with $\alpha = 0.455$ [29]. The normalized biphoton function derived from Eq. (14) is

$$\Phi(\Omega_s, \Omega_i) = \left(\frac{\alpha T_0 DL}{\sqrt{2\pi}} \right)^{1/2} \exp \left[-\frac{(\Omega_s + \Omega_i)^2 T_0^2}{2} \right] \times \exp \left[-\frac{\alpha^2 (DL)^2}{16} (\Omega_s - \Omega_i)^2 \right]. \quad (15)$$

$|\Phi(\Omega_s, \Omega_i)|^2$ yields the probability to detect a signal photon at frequency $\omega_s^0 + \Omega_s$ in coincidence with an idler photon at frequency $\omega_i^0 + \Omega_i$.

The degree of entanglement depends on the ratio between the bandwidth of the pump beam and the bandwidth of down-conversion: $\gamma = \alpha DL / (2\sqrt{2}T_0)$. For $\gamma = 1$ we can write the quantum state as $\Phi(\Omega_s, \Omega_i) = \Phi_s(\Omega_s) \Phi_i(\Omega_i)$, the state is separable. The degree of entanglement is high if $\gamma \gg 1$ or $\gamma \ll 1$ [22, 30]. Figures 3(a), (b) and (c) plot $|\Phi(\Omega_s, \Omega_i)|^2$ for a crystal length $L = 5$ mm and three different pump pulse widths that

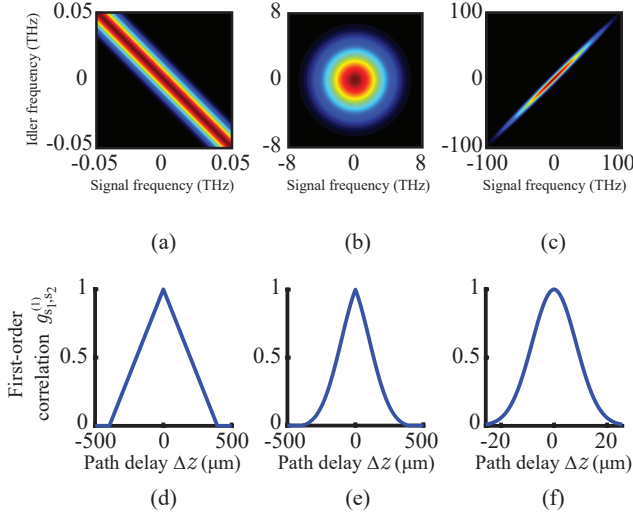


FIG. 3. (a), (b) and (c): Normalized biphoton function $|\Phi(\Omega_s, \Omega_i)|^2$. The axis correspond to angular frequency deviation Ω_s and Ω_i . (d), (e) and (f): First-order correlation function. The pump pulse durations T_0 are: (a) and (d) $T_0 = 100$ ps; (b) and (e) $T_0 = 212$ fs; (c) and (f) $T_0 = 10$ fs. The nonlinear crystal length is $L = 5$ mm.

correspond to $\gamma \ll 1$ ($T_0 = 100$ ps), $\gamma = 1$ ($T_0 = 212$ fs) and $\gamma \gg 1$ ($T_0 = 10$ fs).

When $T_0 \gg DL$ [Fig. 3(a)] there is frequency anti-correlation between signal and idler photons. One can detect coincidences if $\Omega_i \sim -\Omega_s$. For $T_0 \ll DL$ [Fig. 3(c)] there is frequency correlation, there are coincidences only if $\Omega_i \sim \Omega_s$. In between, the degree of correlation is low and the quantum state can become separable [Fig. 3(b)]. Figures 3(d), (e) and (f) show the first-order correlation function corresponding to these cases. For all values of the degree of entanglement we observe coherence, ruling out that the entanglement nature of the paired photons is responsible for the existence of induced coherence.

III. OPTICAL COHERENCE TOMOGRAPHY WITH LARGE BANDWIDTH AND HIGH PHOTON FLUX

OCT is an optical imaging technique that permits cross-sectional and axial high-resolution tomographic

imaging [31]. The axial and transverse resolutions are independent. To obtain information in the axial direction (along the beam propagation), OCT uses a source of light with large bandwidth that allows optical sectioning of the sample.

Different OCT schemes that make use of biphoton sources have been demonstrated. In all cases one photon of the pair probe the sample. Some schemes measure the second-order correlation function of signal and idler photons [32, 33], others measure the first-order correlation function of signal photons generated in different biphoton sources [15, 16] and others measure the flux of signal photons generated in an $SU(1,1)$ nonlinear interferometer [9, 17].

Figures 2 and 3 demonstrate that one can observe induced coherence independently of the degree of entanglement between signal and idler beams. This has an important consequence for the further development of OCT based on nonlinear interferometers. Equation (9) shows that the photon flux generated increases with the nonlinear crystal length. However, for CW pumping, Δ_{dc} goes as $\sim 1/DL$. OCT with high axial resolution requires a large bandwidth. Therefore high axial resolution implies the generation of low photon fluxes and so longer integration times to obtain high-quality images. This is detrimental for OCT applications.

The first-order correlation function is the measure of axial resolution in an OCT system. Equation (11) shows that one can obtain a narrow first-order correlation function, and thus high axial resolution, even for long nonlinear crystal by using an ultrashort pump pulse.

In order to show this effect, we consider a bilayer sample characterized by a reflectivity $r(\Omega) = r_0 + r_1 \exp[i(\omega^0 + \Omega)\tau]$. The delay is $\tau = 2d_0n_0/c$ where d_0 and n_0 designate the thickness and refractive index, respectively, of the sample. The coefficient r_0 is the Fresnel coefficient for the first layer, whereas r_1 is the effective coefficient for the second layer, taking into account propagation through the sample. z_2 is the distance traveled by the idler beam reflected from the first layer, while $z_2 + 2n_0d_0$ is the optical distance traveled by the idler beam reflected from the second layer.

The signal detected at one output port of the beam splitter is

$$N = N_{s1} \left\{ 1 + r_0 g_{s1,s2}^{(1)}(T_1, T_2) \sin \left[(\omega_p^0/c)(z_{p2} - z_{p1}) - (\omega_i^0/c)(z_2 + n_i L) - (\omega_s^0/c)(z_1 - z_3) \right] \right. \\ \left. + r_1 g_{s1,s2}^{(1)}(T'_1, T'_2) \sin \left[(\omega_p^0/c)(z_{p2} - z_{p1}) - (\omega_i^0/c)(z_2 + n_i L + 2n_0 d_0) - (\omega_s^0/c)(z_1 - z_3) \right] \right\}, \quad (16)$$

where $T'_1 = T_1 + \tau$ and $T'_2 = T_2 - \tau$. T_1 and T_2 are given by Eqs. (12) and (13). We can choose $z_{p2} = z_{p1} + cN_i L + z_2$.

Figure 4 shows the photon flux N as a function of Δz

[Eq. (16)] for a 20 μm glass slab (refractive index $n_0 = 1.5$) embedded between air ($n_1 = 1$) and water ($n_2 = 1.3$). We consider three scenarios. Fig. 4(a) considers a

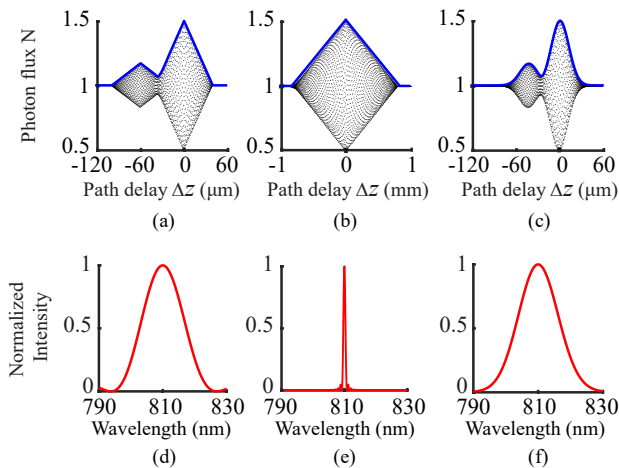


FIG. 4. (a), (b) and (c): Signal N in one output port of the beam splitter as a function of Δz . (a) $L = 0.5 \text{ mm}$, $T_0 = 100 \text{ ps}$, (b) $L = 10 \text{ mm}$, $T_0 = 100 \text{ ps}$, and (c) $L = 10 \text{ mm}$, $T_0 = 100 \text{ fs}$. (d), (e) and (f): Normalized spectrum of the signal photon. The bandwidths (FWHM) are 14.8 nm, 0.8 nm and 20 nm.

pump beam with $T_0 = 100 \text{ ps}$ (quasi CW) and a crystal with $L = 0.5 \text{ mm}$. The interferogram shows two maxima separated by $60 \mu\text{m}$, the sample's optical path length $c\tau$.

Figure 4(b) considers the same pulse duration but $L = 10 \text{ mm}$. The interferogram cannot resolve the thickness of the sample, there is not enough axial resolution. Figure 4(c) considers the same length $L = 10 \text{ mm}$ but now with $T_0 = 100 \text{ fs}$. The interferogram recovers the two maxima, thereby resolving the layers of the sample. The two maxima are separated by $42 \mu\text{m}$, which is smaller than the sample's optical thickness. This result can be understood noticing that the peak of the interferogram when the shape of the first-order correlation function is dominated by the Gaussian function will take place for a value of T_1 [see Eq. (11)]

$$\begin{aligned} \left(1 - \frac{2D_+}{D}\right)(T_1 + \tau) - 2\tau &= 0, \\ \Rightarrow T_1 &= \frac{D + 2D_+}{D - 2D_+}\tau. \end{aligned} \quad (17)$$

Taking into account the values of $D = -263 \text{ fs/mm}$ and $D_+ = 780 \text{ fs/mm}$, the factor $(D + 2D_+)/(D - 2D_+) = -0.71$. The separation between the two maxima corresponding to the two layers is $-0.71 \times 60 \mu\text{m} \sim -42 \mu\text{m}$. This result is reminiscent of the fact that after reflection from the sample, we have two pulses separated by

τ that are injected in the second nonlinear crystal and both show certain delay with the pump pulse [34]. For a case with $D_+ = 0$ we would have again $T_1 = \tau$ as in the quasi CW case.

Figure 4 also shows the signal spectrum for each case, given by $S(\Omega_s) = \int d\Omega_i |\Phi(\Omega_s, \Omega_i)|^2$. The interferograms and spectra show the reciprocal relation between spectral bandwidth and axial resolution.

IV. CONCLUSIONS

We have demonstrated that induced coherence between signal beams generated in separate biphoton sources can be observed independently of the degree of entanglement between signal-idler photon pairs generated in the same nonlinear crystal. In the first demonstration of OCT based on parametric down-conversion, in the high parametric gain regime, the bandwidth of the pump pulse and the bandwidth of down-conversion (0.36 nm) are made comparable due to the use of narrowband filters. However in the high parametric gain one cannot readily quantify signal-idler entanglement.

In the low parametric gain regime, the emission rate of photon pairs increases with the length of the nonlinear crystal, regardless of the duration of the pump pulse. We have shown that an OCT scheme based on induced coherence can achieve high axial resolution and high photon emission rates by combining ultrashort pumping with long crystals. The method maintains its salutary features, i.e., probing the sample with photons centered at the most appropriate wavelength while using the optimum wavelength for photodetectors.

ACKNOWLEDGMENTS

We acknowledge financial support from the Spanish Ministry of Economy and Competitiveness through the Severo Ochoa program for Centres of Excellence in R&D (SEV-2015-0522), from Fundaci Privada Cellex, from Fundaci Mir-Puig, and from Generalitat de Catalunya through the CERCA program. GJM was supported by the Secretaria d'Universitats i Recerca del Departament d'Empresa i Coneixement de la Generalitat de Catalunya, as well as the European Social Fund (L'FSE inverteix en el teu futur)/FEDER. DLM acknowledges funding from Consejo Nacional de Ciencia y Tecnología (293471, 295239, APN2016-3140) and ARS acknowledges support from Becas de Movilidad CONACYT, SEGIB and Fundación Carolina.

-
- [1] X. Y. Zou, L. J. Wang, and L. Mandel, Induced coherence and indistinguishability in optical interference, *Phys. Rev. Lett.* **67**, 318 (1991).
 [2] X. Y. Zou, T. P. Grayson, and L. Mandel, Observation

- of quantum interference effects in the frequency domain, *Phys. Rev. Lett.* **69**, 3041 (1992).
 [3] A. V. Belinsky and D. N. Klyshko, Interference of classical and non-classical light, *Phys. Lett. A* **166**, 303 (1992).

- [4] H. M. Wiseman and K. Mølmer, Induced coherence with and without induced emission, *Phys. Lett. A* **270**, 245 (2000).
- [5] J. H. Shapiro, D. Venkatraman, and F. N. C. Wong, Classical imaging with undetected photons, *Sci. Rep.* **5**, 10329 (2015).
- [6] M. Lahiri, A. Hochrainer, R. Lapkiewicz, G. B. Lemos, and A. Zeilinger, Nonclassicality of induced coherence without induced emission, *Phys. Rev. A* **100**, 053839 (2019).
- [7] M. V. Chekhova and Z. Y. Ou, Nonlinear interferometers in quantum optics, *Adv. Opt. Photonics* **8**, 104 (2016).
- [8] G. B. Lemos, V. Borish, G. D. Cole, S. Ramelow, R. Lapkiewicz, and A. Zeilinger, Quantum imaging with undetected photons, *Nature* **512**, 409 (2014).
- [9] A. Cardoso, L. P. Berrueto, D. F. Ávila, G. B. Lemos, W. M. Pimenta, C. H. Monken, P. L. Saldanha, and S. Pádua, Classical imaging with undetected light, *Phys. Rev. A* **97**, 033827 (2018).
- [10] M. Kutas, B. Haase, P. Bickert, F. Riechinger, D. Molter, and G. von Freymann, Terahertz quantum sensing, *Sci. Adv.* **6**, eaaz8065 (2020).
- [11] D. A. Kalashnikov, A. V. Paterova, S. P. Kulik, and L. A. Krivitsky, Infrared spectroscopy with visible light, *Nat. Photonics* **10**, 98 (2016).
- [12] A. V. Paterova, H. Yang, D. Kalashnikov, and L. Krivitsky, Measurement of infrared optical constants with visible photon, *New J. Phys.* **20**, 043015 (2018).
- [13] I. Kviatkovsky, H. M. Chrzanowski, E. G. Avery, H. Bartolomaeus, and S. Ramelow, Microscopy with undetected photons in the mid-infrared, *arXiv:2002.05960* (2020).
- [14] A. V. Paterova, M. M. Sivakumar, H. Yang, G. Grenci, and L. A. Krivitsky, Hyperspectral infrared microscopy with visible light, *arXiv:2002.05956* (2020).
- [15] J. Le Gouet, D. Venkatraman, F. N. C. Wong, and J. H. Shapiro, Classical low-coherence interferometry based on broadband parametric fluorescence and amplification, *Opt. Express* **17**, 17874 (2009).
- [16] A. Vallés, G. Jiménez, L. J. Salazar-Serrano, and J. P. Torres, Optical sectioning in induced coherence tomography with frequency-entangled photons, *Phys. Rev. A* **97**, 023824 (2018).
- [17] A. V. Paterova, H. Yang, C. An, D. A. Kalashnikov, and L. A. Krivitsky, Tunable optical coherence tomography in the infrared range using visible photons, *Quantum Sci. Technol.* **3**, 025008 (2018).
- [18] A. Vanselow, P. Kaufmann, I. Zorin, B. Heise, H. Chrzanowski, and S. Ramelow, Mid-infrared frequency-domain optical coherence tomography with undetected photons, in *Quantum Information and Measurement* (Optical Society of America, 2019) pp. T5A–86.
- [19] C. You, S. Adhikari, X. Ma, M. Sasaki, M. Takeoka, and J. P. Dowling, Conclusive precision bounds for SU(1,1) interferometers, *Phys. Rev. A* **99**, 042122 (2019).
- [20] N. R. Miller, S. Ramelow, and W. N. Plick, Super-sensitive metrology using induced coherence, *arXiv:1907.09004* (2020).
- [21] B. Dayan, Theory of two-photon interactions with broadband down-converted light and entangled photons, *Phys. Rev. A* **76**, 043813 (2007).
- [22] S. Parker, S. Bose, and M. B. Plenio, Entanglement quantification and purification in continuous-variable systems, *Phys. Rev. A* **61**, 032305 (2000).
- [23] X. Y. Zou, T. Grayson, G. A. Barbosa, and L. Mandel, Control of visibility in the interference of signal photons by delays imposed on the idler photons, *Phys. Rev. A* **47**, 2293 (1993).
- [24] W. Wasilewski, A. I. Lvovsky, K. Banaszek, and C. Radzewicz, Pulsed squeezed light: Simultaneous squeezing of multiple modes, *Phys. Rev. A* **73**, 063819 (2006).
- [25] J. P. Torres, K. Banaszek, and I. A. Walmsley, Engineering nonlinear optic sources of photonic entanglement, *Progress in Optics* **56**, 227 (2011).
- [26] H. A. Haus, *Electromagnetic noise and quantum optical measurements*, Springer Verlag (2000).
- [27] R. W. Boyd, G. S. Agarwal, C. Chan, K. Wai, A. K. Jha, and M. N. O'Sullivan, Propagation of quantum states of light through absorbing and amplifying media, *Opt. Comm.* **281**, 3732 (2008).
- [28] Data taken from Covesion Ltd., <https://www.covesion.com>.
- [29] C. I. Osorio, A. Valencia, and J. P. Torres, Spatiotemporal correlations in entangled photons generated by spontaneous parametric down conversion, *New J. Phys.* **10**, 113012 (2008).
- [30] M. Hendrych, X. Shi, A. Valencia, and T. J. P., Broadening the bandwidth of entangled photons: A step towards the generation of extremely short biphotons, *Phys. Rev. A* **79**, 023817 (2009).
- [31] D. Huang, E. A. Swanson, C. P. Lin, J. S. Schuman, W. G. Stinson, W. Chang, M. R. Hee, T. Flotte, K. Gregory, C. A. Puliafito, and J. G. Fujimoto, Optical coherence tomography, *Science* **254**, 1178 (1991).
- [32] M. B. Nasr, B. E. A. Saleh, A. V. Sergienko, and M. C. Teich, Demonstration of dispersion-canceled quantum-optical coherence tomography, *Phys. Rev. Lett.* **91**, 083601 (2003).
- [33] D. Lopez-Mago and L. Novotny, Quantum-optical coherence tomography with collinear entangled photons, *Opt. Lett.* **37**, 4077 (2012).
- [34] Y.-H. Kim, M. Chekhova, S. Kulik, Y. Shih, and M. Rubin, First-order interference of nonclassical light emitted spontaneously at different times, *Phys. Rev. A* **61**, 051803 (2000).